JOURNAL OF MATERIALS SCIENCE 32 (1997) 2077–2086

Fracture mechanisms in a stoichiometric $3Al_2O_32SiO_2$ mullite

C. BAUDÍN
Instituto de Cerámica y Vidrio (CSIC), E-28500, Arganda del Rey, Madrid, Spain

The mechanical behaviour from room temperature up to 1400 °C (strength, toughness, Young's modulus) of a $3Al_2O_3 \cdot 2SiO_2$ dense mullite material containing 0.2 wt % alkali has been studied. Microstructure has been characterized by scanning electron microscopy (SEM) and transmission electron microscopy (TEM). Toughness, bend strength and static Young's modulus have been determined from room temperature up to 1400 °C. The influence of strain rate on fracture behaviour has been investigated and a correlation of the mechanical parameters to fractographic observations by SEM has been stated. A strong influence of loading rate on microstructural modifications during fracture at 1300 °C has been found.

1. Introduction

During the last decade, several methods to obtain highly reactive, homogeneous and pure mullite powders have been developed [1, 2, 3]. In these powders there are always small amounts of impurities whose nature depends on the synthesis route. When powders are obtained by sol–gel methods the main contaminants come from milling after mullite crystallization and mullite powders obtained from natural raw materials contain alkalis and alkaline-earths. Impurities such as iron oxide or titania [4], that enter in solid solution in mullite in rather large quantities or zirconia, which remain as isolated particles in the material [5], do not degrade mechanical properties at high temperature. Conversely other impurities such as alkaline oxides strongly affect the high-temperature mechanical behaviour of the material as they form liquids at rather low temperatures (eg. $T \sim 1000\,^{\circ}C$ for Na_2O [6]) which remain as glassy phases after sintering. Softening temperature and viscosity of these residual amorphous phases are determined by their composition [7, 8]. Moreover, quantity and distribution in the microstructure of these remaining phases depend on sintering temperature and content and nature of impurities.

From a mechanical point of view, the most studied property of mullite materials at high temperature has been creep [9–13]. A variety of mechanisms, from solid state diffusion to viscous flow, and activation energies, ranging from $500\,kJ\,mol^{-1}$ [9, 10] to $1300\,kJ\,mol^{-1}$ [11], have been reported for stoichiometric mullite creep. This diversity in data, in spite of the similar ranges of test temperatures and loads, could be attributed to slight differences in impurity content and nature as small amounts of additives greatly change not only the viscosity of liquids [7, 8] but also their wetting characteristics and, thus, their distribution in the microstructure.

Fracture mechanics parameters in mullite have been less analysed, probably due to its inherent brittleness. Little attention has been paid to fracture mechanisms and most of the work has been devoted to establish relationships between mullite stoichiometry or microstructure and parameters such as toughness and modulus of rupture [14–24]. In most conventionally sintered high purity 3 : 2 stoichiometric mullites, in which very little or no glassy phase is detected, bend strengths between 250 and 400 MPa at room temperature are reported and these values are maintained up to temperatures ranging from 1200 to 1400 °C [11, 16, 18, 20, 24]. This mechanical behaviour is usually claimed as being linear elastic and, consequently, not affected by the presence of remaining glassy phases [16, 18, 20]. But, in linear elastic materials a decrease of Young's modulus with temperature due to elastic bond relaxation is expected and mechanical properties should decrease accordingly, as reported for a highly pure mullite [21]. Then, some kind of viscous phenomena must take place in the materials whose room temperature bend strength values are maintained at high temperature, even though no peak in strength is detected, as in other mullite materials in which softening of the glassy phase is considered to be responsible for their behaviour [14, 22, 24]. When viscous phenomena take place an influence of loading rate on the values of the mechanical parameters is expected.

In the present work, the mechanical behaviour of a stoichiometric $3Al_2O_3 \cdot 2SiO_2$ mullite material containing alkaline impurities has been studied. The selected parameters have been toughness, bend strength, stress–strain relations and Young's modulus. The influence of temperature and strain rate on these parameters has been studied, paying special attention to correlate the parameter trends to the aspect of the fracture surfaces.

0022–2461

2. Experimental procedure

A mullite material has been prepared from commercial powders. The starting powders are coarse grained (1.8 μm) and were attrition milled with mullite balls (down to 0.8 μm) before isostatically pressing (200 MPa) and sintering at 1630 °C for 4 h.

In order to determine the amount of alkalis in the remaining glass five samples ($3 \times 4 \times 50\ mm^3$), machined from the sintered blocks, were etched with HF and the obtained solution was chemically analysed.

Polished and thermally etched (1500 °C) samples were observed with a scanning electron microscope (SEM). Grain size distributions were obtained by image analysis of 150 grains in SEM micrographs (Imagist PGT). The diameter of the particles, assumed spherical, was calculated as that of the equivalent area. For transmission electron microscope (TEM) observations, specimens were thinned, dimpled and Ar milled. Density was determined by Archimedes' method, using distilled water.

All samples for mechanical testing were diamond machined from sintered mullite blocks. Room temperature dynamic Young's modulus was obtained from the resonance frequency of $3 \times 4 \times 50$ mm bars. For bend strength and static Young's modulus measurement bars of $4 \times 3 \times 50\ mm^3$ were used, bend strength bars were polished and chamfered after machining. For toughness measurements, single edge notched beam (SENB), bars of $4 \times 6 \times 50\ mm^3$ were used and notches of about 3 mm long and 25 μm width were introduced with a fine diamond disc.

For mechanical tests, four-point bending fixtures (20–40 mm, inner–outer span) made of steel, SiC or Al_2O_3 for room temperature, 800–1000 °C and 1100–1400 °C, respectively were used. Tests at 800 and 1000 °C were also performed with the Al_2O_3 supports to check their equivalence to the SiC ones. A universal load testing machine (Instron 8600) with an electrically heated furnace was used for all tests.

For bend strength measurements loading rates from 10 to 1000 N min^{-1} were used. For K_{IC} measurements the actuator travelled at different rates ranging from 0.005 to 5 mm min^{-1}. Reported values of bend strength and K_{IC} are the average of at least five measurements.

Strain of the bend bars was calculated from their central point deflection measured using a SiC probe attached to a linear variable displacement transducer (LVDT) through an alumina tube. For stress–strain relations at different temperatures samples were loaded at 1000 N min^{-1} four times up to a load about 50% of the average fracture load. Identical curves were obtained after the first load cycle and the lower slope of the first cycle was attributed to the setting of the LVDT system. Static Young's modulus was calculated from the stress–strain relations of the second load cycle and reported values are the average of three measurements. Additional stress–strain relations were obtained at 1300 °C for loading rates 10–100 N min^{-1}. Fracture surfaces of the bend strength and toughness samples were observed by a scanning electron microscope (SEM).

3. Results

Chemical analysis of the milled powder is shown in Table I, total alkali ($Na_2O + K_2O$) is about 0.2 wt %. General properties of the sintered material are collected in Table II. The analysis of the remaining glass are summarized in Table III. Alkaline content in the remaining glass is larger than in the average composition of the powder.

Fig. 1 shows the microstructure of the studied mullite material. It has a fine microstructure and porosity is mainly intergranular (Fig. 1a). Remaining glass was scarcely observed and it always located at triple grain junctions (Fig. 1b), being alkaline impurities concentrated at those glassy areas as energy dispersive X-ray (EDX) analysis revealed (Table III). At the level of resolution employed no glassy phase films were observed along grain boundaries in any sample.

In Fig. 2 characteristic stress-strain relations are depicted. When a loading rate of 1000 N min^{-1} was used, linear relations were obtained at all temperatures (Fig. 2a). For loading rates of 100 and 10 N min^{-1} linearity was lost at 0.0004 and 0.00035 strain respectively in samples tested at 1300 °C (Fig. 2b). No lack of linearity was found in samples tested at room temperature at any loading rate.

Young's modulus values are summarized in Fig. 3. For the highest loading rate, a steady decrease takes place as testing temperature increases (Fig. 3a). Room temperature Young's modulus does not vary with loading rate (Fig. 3b) and is lower than the dynamic one (Table II). When the linear part of the

TABLE I Chemical analysis of the milled powder

	(wt %)
Ignition loss	1.66
SiO_2	25.98
Al_2O_3	71.52
Fe_2O_3	0.10
TiO_2	0.006
Na_2O	0.18
K_2O	0.017
Zr_2O	0.02
Y_2O_3	n.d.
CaO	0.082
MgO	0.02

TABLE II Characteristics of the studied material

Dynamic Young's modulus (GPa)	Density (g cm^{-3})	Average grain size (μm)
195 ± 4	3.01 ± 0.02	0.7 ± 0.5

TABLE III Remaining glass analysis

Chemical analysis	TEM–EDX analysis
Mass loss in HF = 0.23 wt %	
K_2O in extracted glass = 0.8 wt %	K_2O = 0.4 wt %
Na_2O in extracted glass = 2.3 wt %	Na_2O = 1.5 wt %

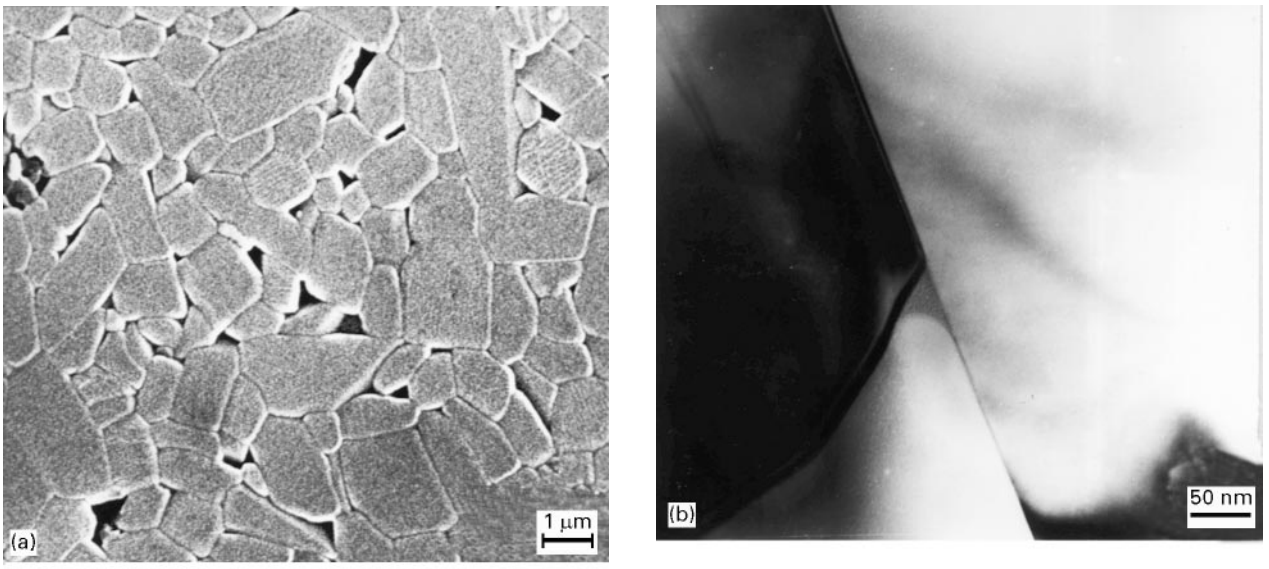

Figure 1 Microstructure of the studied mullite material. (a) SEM, polished and thermally etched (1500 °C, 1 h) surface. (b) TEM, ion thinned sample.

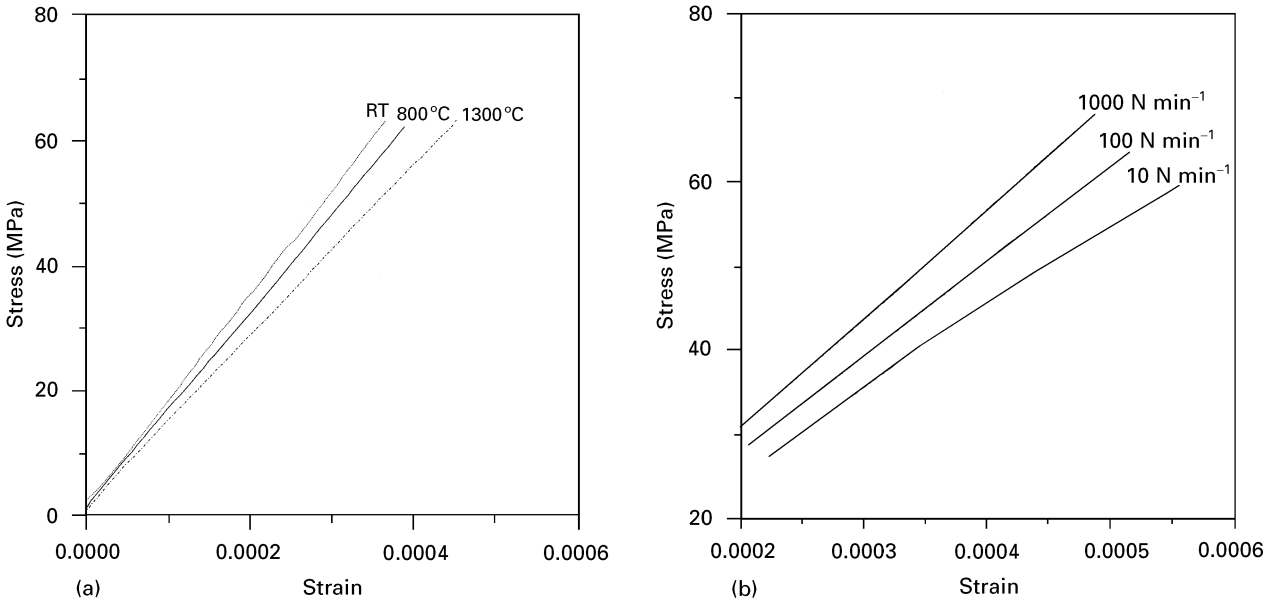

Figure 2 Characteristic stress–strain relations. (a) Effect of temperature. Loading rate = 1000 N min^{-1}. ····, RT; ——800 °C; —·— 1300 °C. (b) Effect of loading rate at 1300 °C.

stress–strain curves obtained at 1300 °C (Fig. 2b) is adjusted, an increase in Young's modulus as loading rate increases is found (Fig. 3b).

Bend strength values are depicted in Fig. 4. Values obtained using the highest loading rate decrease from room temperature to 800 °C and from this temperature an increase up to a peak in strength at 1200 °C is observed (Fig. 4a). Variations of bend strength with loading rate are always inside the experimental variability at room temperature as well as at 1300 °C (Fig. 4b).

In Fig. 5, characteristic fracture surfaces of bend bars are shown. Critical defects were large ($\approx$ 25–40 μm) isolated pores (Fig. 5a) or zones ($\approx$ 100 μm) of coalescence of smaller pores (Fig. 5b). In some samples tested at 1300 °C using a loading rate of 10 N min^{-1} critical defects were surrounded by zones of subcritical crack growth pattern, such as the one shown in Fig. 6.

Toughness values obtained using an actuator speed of 0.05 mm min^{-1} as a function of temperature are represented in Fig. 7a. A decrease from room temperature up to 800 °C followed by a slight increase for temperatures from 1000 to 1200 °C is observed. Maximum value is maintained from 1200 to 1400 °C.

Fig. 7b shows K_{IC} data as a function of the actuator speed for tests performed at room temperature and 1300 °C. At room temperature, average K_{IC} values remain constant and variability decreases as actuator speed increases. At 1300 °C, a non-monotonous dependence of toughness on actuator speed is observed: maximum values are obtained using the slowest speed (0.005 mm min^{-1}) and a minimum is found for a speed of 0.01 m min^{-1}.

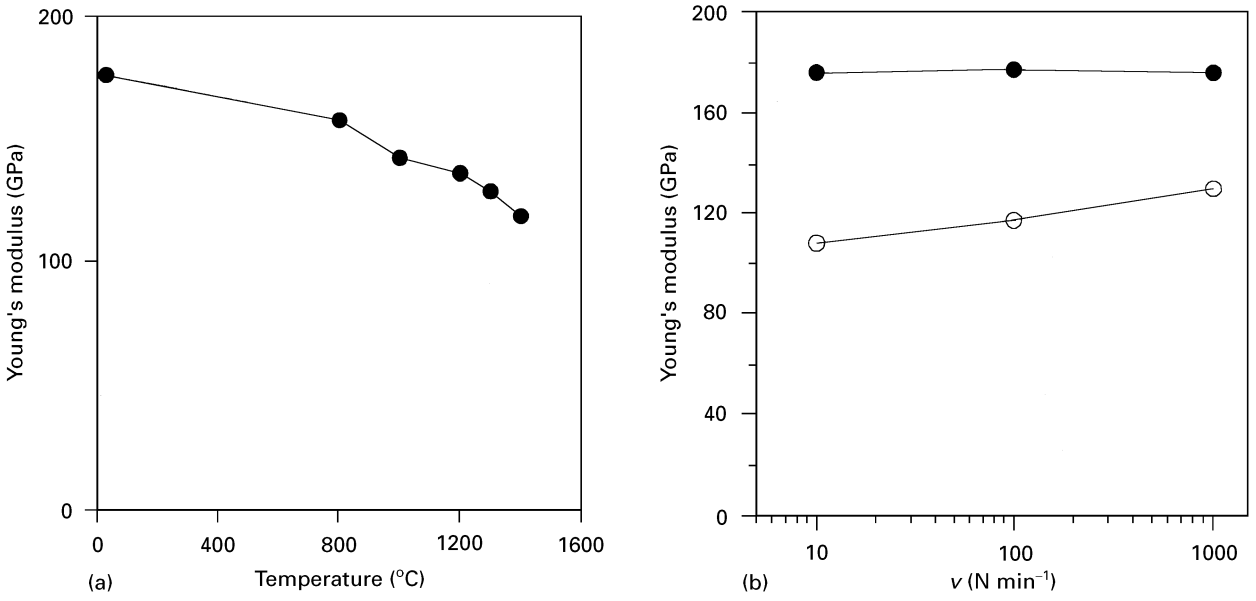

Figure 3 Young's modulus. (a) Effect of temperature. Loading rate = 1000 N min^{-1}. (b) Effect of loading rate at room temperature (●) and 1300 °C (○).

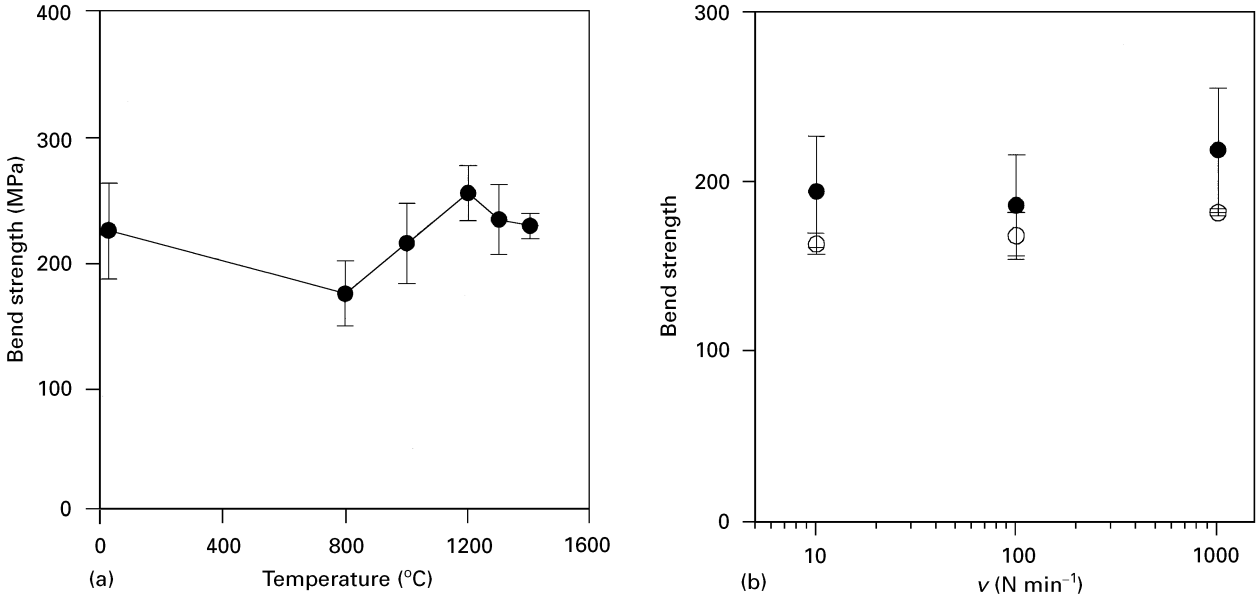

Figure 4 Bend strength. (a) Effect of temperature. Loading rate = 1000 N min^{-1}. (b) Effect of loading rate at room temperature (●) and 1300 °C (○).

No special features were observed in the fracture surfaces of toughness samples tested at room temperature, the fracture being mainly transgranular through the specimen. Characteristic fracture surfaces of notched bars after toughness testing at 1300 °C are collected in Figs 8 and 9. Differentiated zones close to the notch were found in the samples tested using actuator speeds lower than 5 mm min^{-1} (Fig. 8a–c). Most of these zones had a semicircular shape as the ones shown in Fig. 8a, b, being their size minimum for samples tested at 0.005 mm min^{-1}. Some of these zones were made of several distinct areas as the one shown in Fig. 8c and no correlation of their size to loading rate was possible in these cases. Higher magnification (Fig. 9) reveals a sharp transition from intergranular to transgranular fracture at the boundary of these zones (Fig. 9a) in which significant cavitation is observed. Far from the notch transgranular fracture patterns were found in all the samples (Fig. 9c). In the samples tested using the lowest loading rates, partial dissolution of the grains located in the areas close to the subcritical–critical interphase was observed (Fig. 10). No special features were observed for samples tested at 5 mm min^{-1} (Fig. 8d).

4. Discussion

4.1. Microstructure

The mullite studied here has a fine microstructure with a majority of grains being equiaxed (Fig. 1a, Table II).

No glassy films along grain boundaries were observed with the available techniques, but the small angles formed by the glassy pockets at triple points

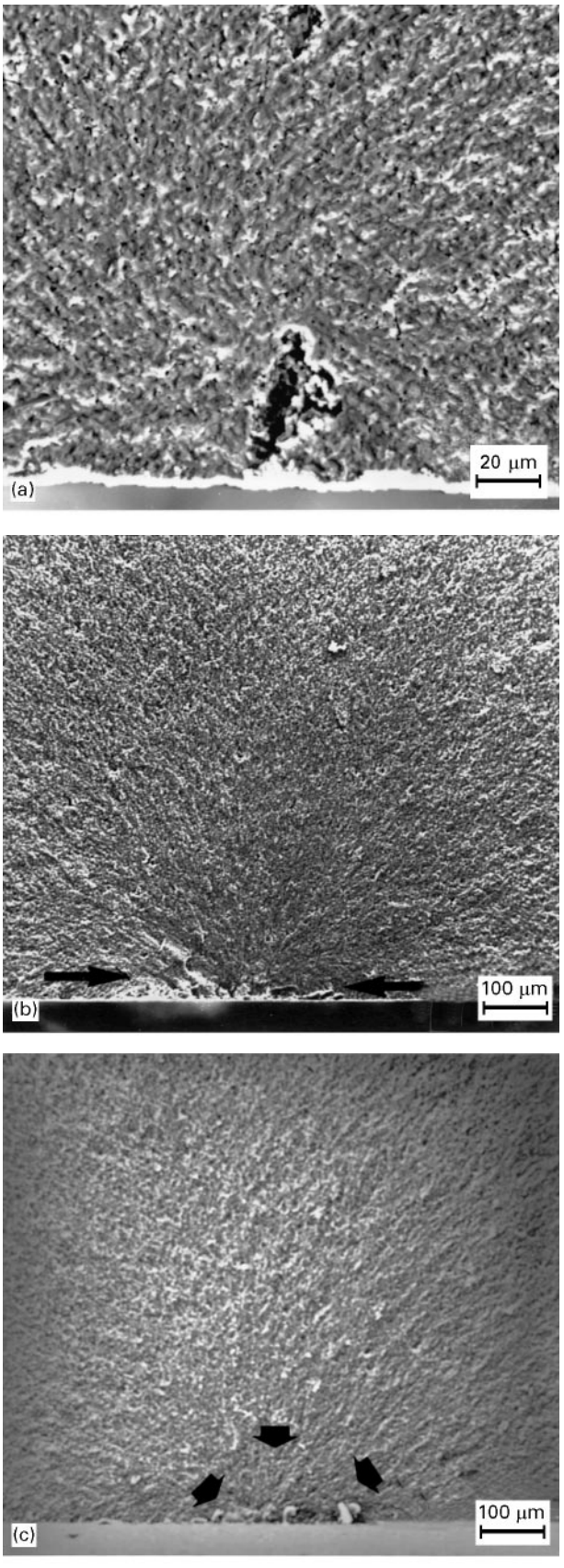

Figure 5 Characteristic critical defects in fracture surfaces (SEM) of bend strength bars. (a) Pores. Sample tested at room temperature using a loading rate of 1000 N min^{-1}. Bend strength = 263 MPa. (b) Coalescence of pores. Sample tested at 1000 °C using a loading rate of 1000 N min^{-1}. Bend strength = 210 MPa. (c) Coalescence of pores. Sample tested at room temperature using a loading rate of 10 N min^{-1}. Bend strength = 202 MPa.

(Fig. 1b) indicate that at least partial penetration of the liquid has occurred. Moreover, thin glassy films of ≈ 10 nm at mullite–mullite interfaces have been observed by other authors by high resolution TEM (HRTEM) in highly pure stoichiometric materials [13, 24].

The amount of alkalis ($Na_2O + K_2O$) in the remaining glass determined by TEM–EDX is lower than the amount determined by chemical analysis of the solution (Table III). This last value must be closer to reality as EDX data are masked by the surrounding crystalline mullite. Even though the amount of alkalis in the average composition of the material is rather low (Table I), the concentration of these compounds in the remaining glass, determined by both methods, is large ($\times 9.5$, $\times 15.5$ for chemical analysis and EDX, respectively, Table III). This glass will have low viscosity at high temperatures due to the concentration of the alkaline impurities in it. For example, a silica glass with 3.5 wt % Na_2O has a viscosity of about 10^7 dPa at 1300 °C, which is in the working range of the glass [8]. In this range, viscosity of glasses maintained at a certain temperature diminish with exposure time and stress. The glass in the material considered here ($Na_2O + K_2O = 3.1$ wt %) might have a still lower viscosity due to the presence of small amounts of Al_2O_3.

4.2. Room temperature mechanical behaviour

Room temperature dynamic Young's modulus (Table II) is lower than that reported by other authors (246, 224 GPa [17, 11]), and, as expected, is larger than the static one (Fig. 3). Room temperature bend strength and toughness values are in the average of those reported for conventionally sintered stoichiometric mullites (250–400 MPa, 2–3 MPa m$^{1/2}$ [3]).

No dependence of stress–strain relations, Young's modulus, bend strength or K_{IC} values on loading rate (Figs 2b, 4b, 7b) and no subcritical crack growth patterns were observed close to the critical defects bend strength specimens (Fig. 5a, c) or close to the notches in toughness specimens tested at room temperature. In fact, room temperature bend strength values (Fig. 4) can be correlated to K_{IC} values (Fig. 7) through the general equation

$$\sigma_f = \frac{Z}{Y}\frac{K_{IC}}{c^{1/2}}$$

Substituting the constant values for a semielliptical ($Z = 1.6$) surface ($Y = 2$) crack or radius c [25] and introducing K_{IC} and σ_f minimum and maximum values into the expression, critical defect sizes ($2c$) ranging from 60 and 200 μm are obtained which agrees with fractographic observations (Fig. 5). It is interesting to note that the range of loading rates that have been used is large, so thus no slow crack growth by stress corrosion takes place in this mullite and it behaves linearly until fracture, as reported for other high purity mullites tested at room temperature in air [15].

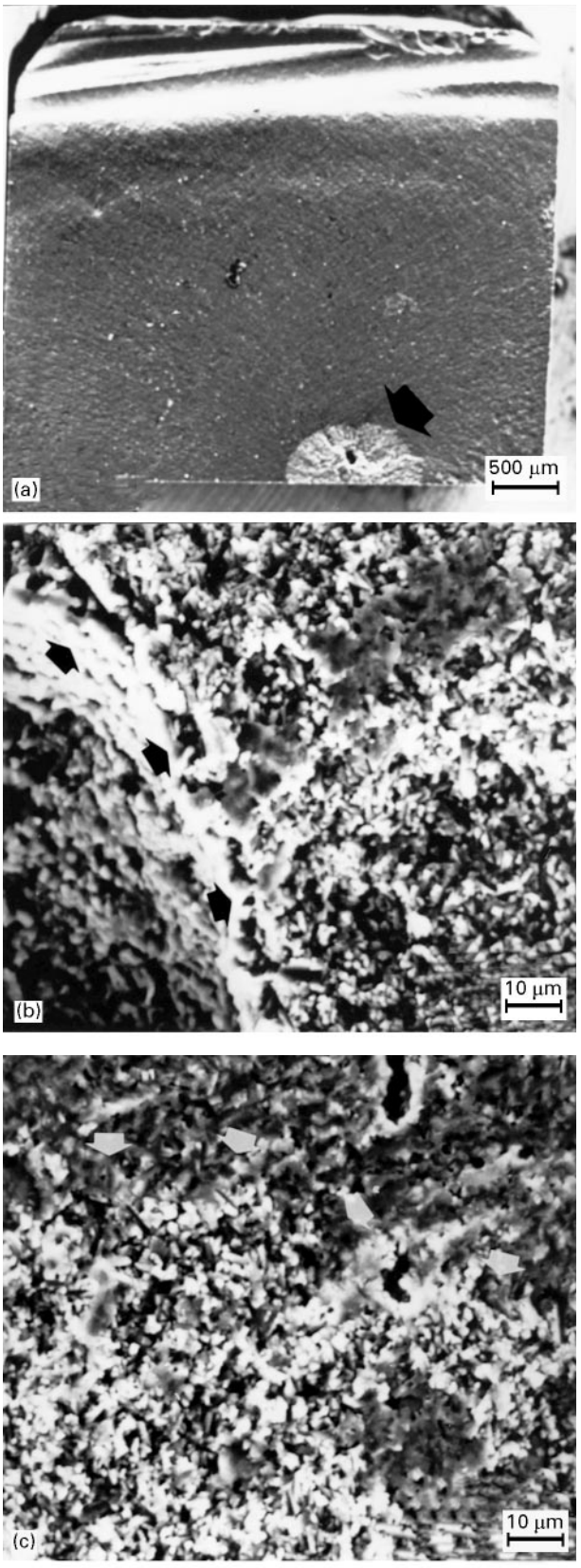

Figure 6 Fracture surface (SEM) of a bend strength sample tested at 1300 °C using a loading rate of 10 N min^{-1}. Bend strength = 156 MPa. (a) General aspect. (b) Defect-subcritical crack growth zone interphase. (c) Subcritical crack growth zone-sample interphase.

4.3. Mechanical behaviour up to 1400 °C

The most striking feature of high temperature mechanical data and fracture patterns in the studied material is their strong dependence on loading conditions.

High temperature bend strengths of a 74 wt % Al_2O_3 mullite, in which no remaining glass was reported, as a function of loading rate have been analysed by Kumazawa *et al.* [21]. In this material and for the range of loading rates used by these authors (0.01–0.5 mm min^{-1}), no dependence of strength data at 1300 °C on loading rate was found. Moreover, a steady decrease of bend strength from room temperature up to 1300 °C occurred.

As discussed in section 4.1, the remaining glass in the material studied here would have a viscosity in its working range and, thus, viscous phenomena implying time and stress intensity dependent properties can be expected. Most ceramics, like the mullite studied here, contain remaining glassy phases that have been formed during sintering. In these materials peak in strength behaviour as testing temperature increases is found, which indicates that non-elastic phenomena contribute to bend strength. In materials such as aluminas, silicon nitride and glass ceramics peaks in strength with temperature have been associated with several phenomena derived from softening of those remaining glassy phases [26–29]. A variety of mechanisms, from blunting of critical flaws to grain boundary sliding, crack branching or formation of crack bridges by viscous flow during crack propagation have been proposed. Moreover, in most materials not a single mechanism takes place but an interaction of several occurs depending on composition and distribution of the glass, testing temperature and strain rate.

As shown in Fig. 2b, the mullite studied here behaves linearly elastic at high temperature when the highest loading rate is used. The decrease in Young's modulus values determined using this rate with temperature (Fig. 3a) is related to the decrease in elastic properties as temperature increases due to elastic bond relaxation. Bend strength values determined using this high rate do not follow the same trend as the temperature increases over 800 °C, following the usual peak in strength behaviour of ceramic materials containing glass (Fig. 4a). Conversely, linearity at 1300 °C is lost as loading rate decreases (Fig. 2b) which reveals the occurrence of non-elastic phenomena during loading at low rates which do not contribute to bend strength values (Fig. 4b). The lack of correlation between Young's modulus values, stress–strain relations and bend strength data indicates that the increase in strength values determined using the highest loading rate as temperature increases is due to viscous phenomena that do not take place during loading such as healing of the critical cracks during heating of the samples. The conclusion agrees with the diminution of variability in strength data of samples tested at 1300 °C (Fig. 4a).

When large defects are found in the fracture surfaces of bend strength samples tested at the lowest loading rates subcritical crack growth zones are observed next to the critical defects (Fig. 6) in which intergranular fracture and cavitation are apparent and a sharp transition to transgranular fracture takes place. This feature was not observed when larger loading rates were used being fracture transgranular through the

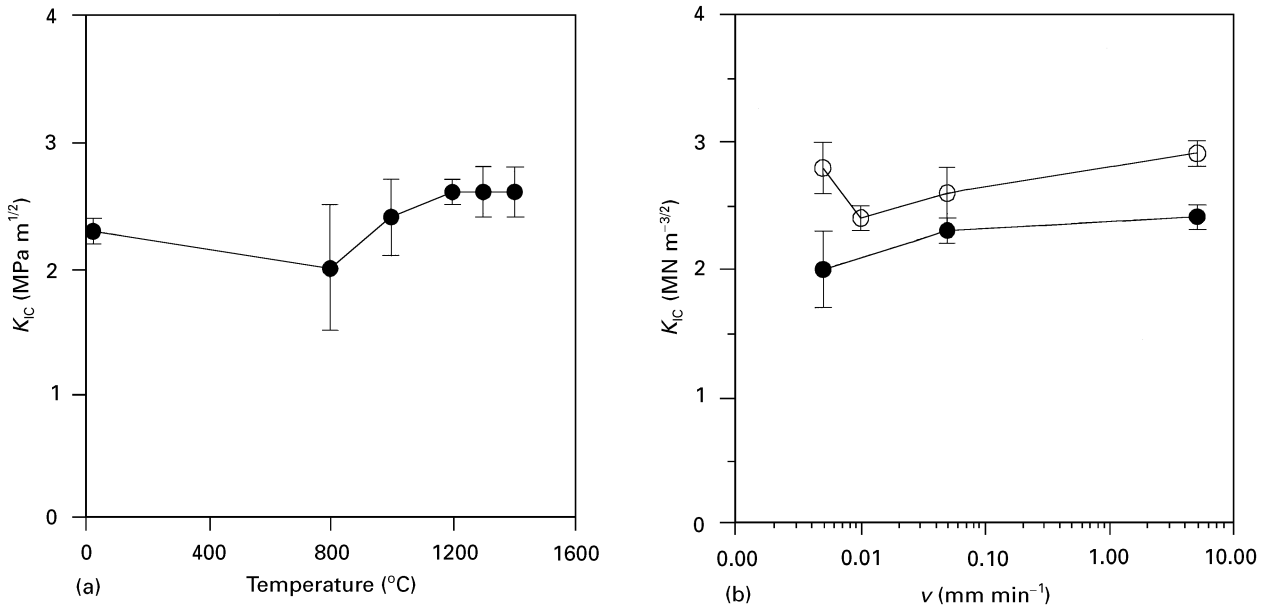

Figure 7 Toughness, K_{IC}. (a) Effect of temperature. Actuator speed = 0.05 mm min^{-1}. (b) Effect of actuator speed at room temperature (●) and 1300 °C (○).

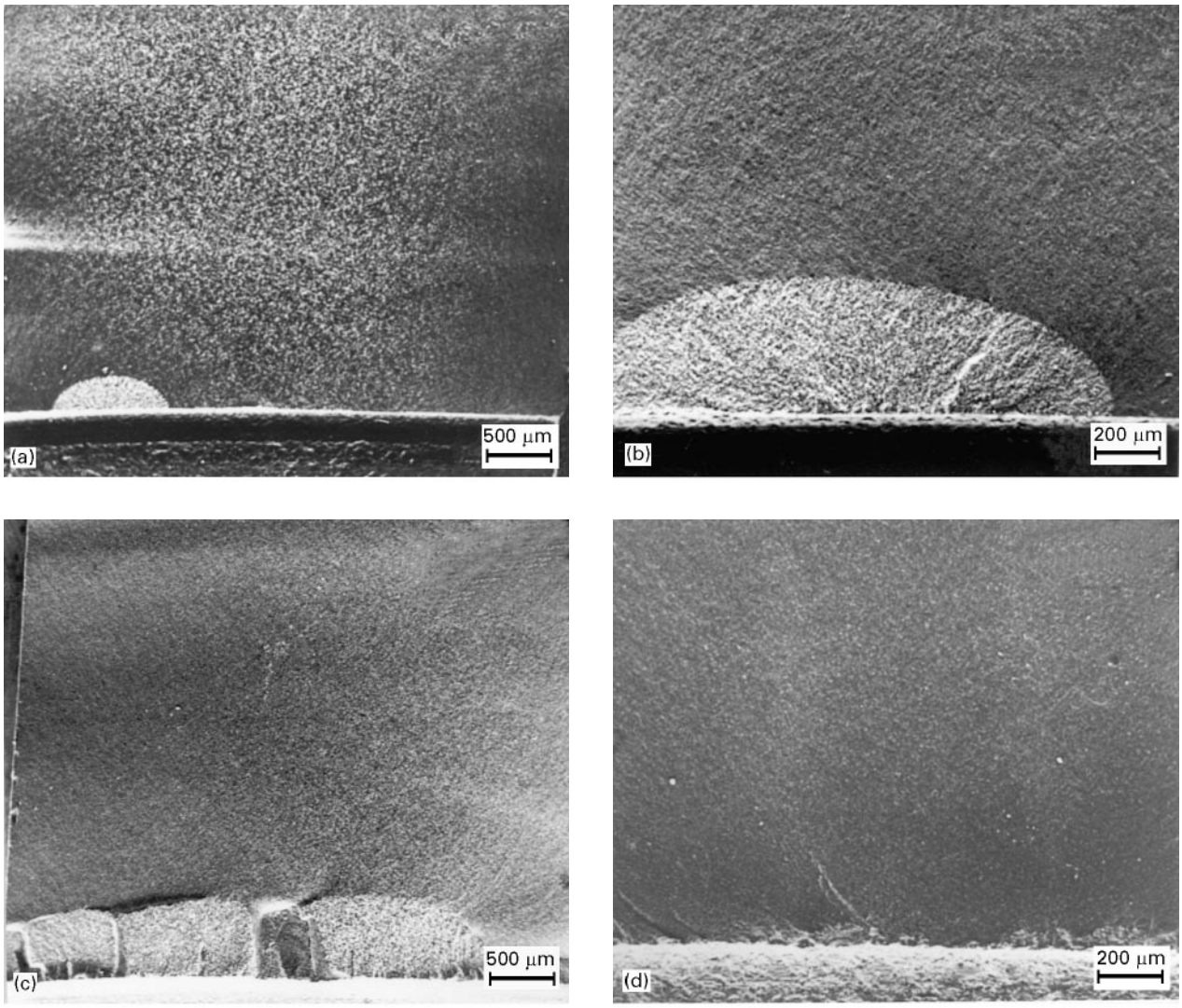

Figure 8 General aspect of characteristic fracture surfaces (SEM) of notched bars after toughness testing at 1300 °C using the following actuator speeds: (a) 0.005 mm min^{-1}, K_{IC} = 2.9 MPa m$^{1/2}$; (b) 0.01 mm min^{-1}, K_{IC} = 2.3 MPa m$^{1/2}$; (c) 0.05 mm min^{-1}, K_{IC} = 2.6 MPa m$^{1/2}$; (d) 5 mm min^{-1}, K_{IC} = 2.9 MPa m$^{1/2}$.

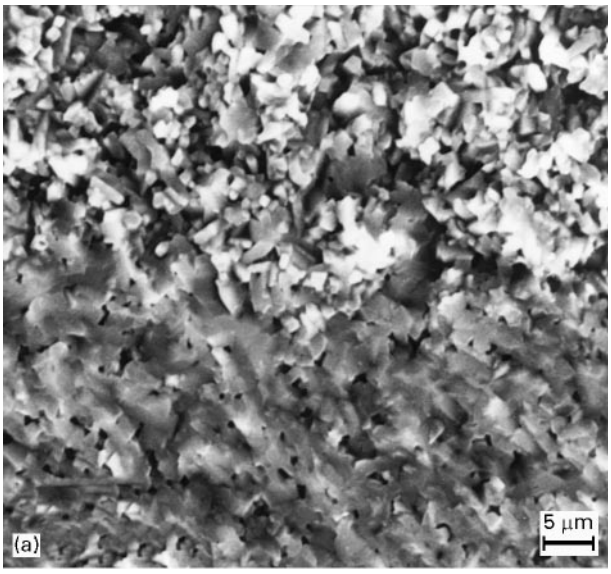

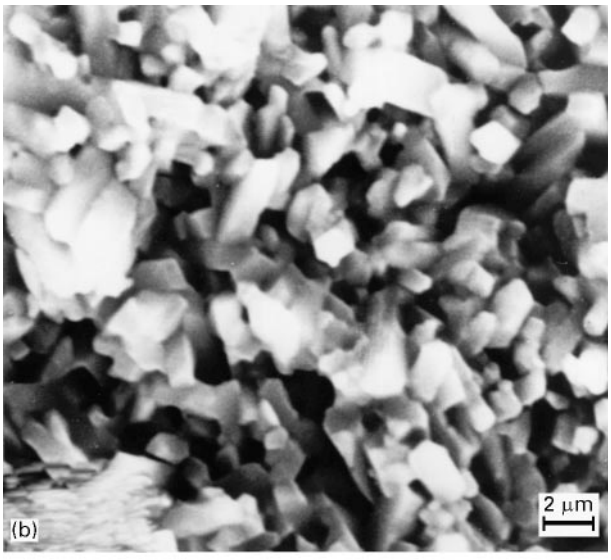

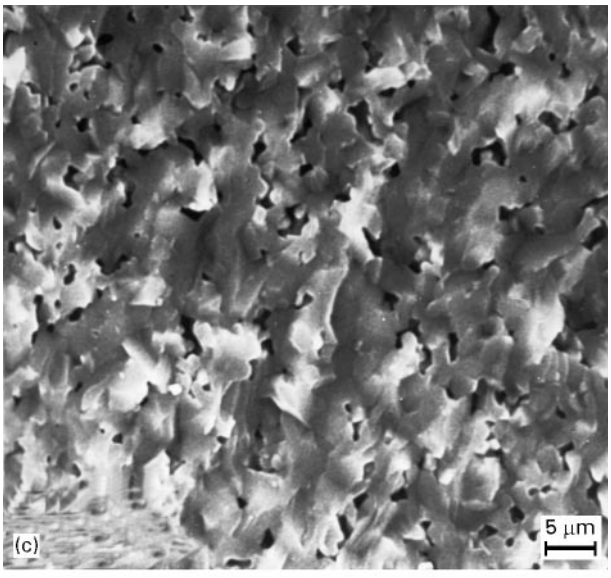

Figure 9 Characteristic features of fracture surfaces of samples tested at 1300 °C. High magnification. (a) Subcritical crack growth zone-sample interphase. Sample tested using an actuator speed of 0.01 mm min^{-1}. (b) Subcritical crack growth zone. Sample tested using an actuator speed of 0.01 mm min^{-1}. (c) Critical fracture far from the notch. Sample tested using an actuator speed of 0.005 mm min^{-1}.

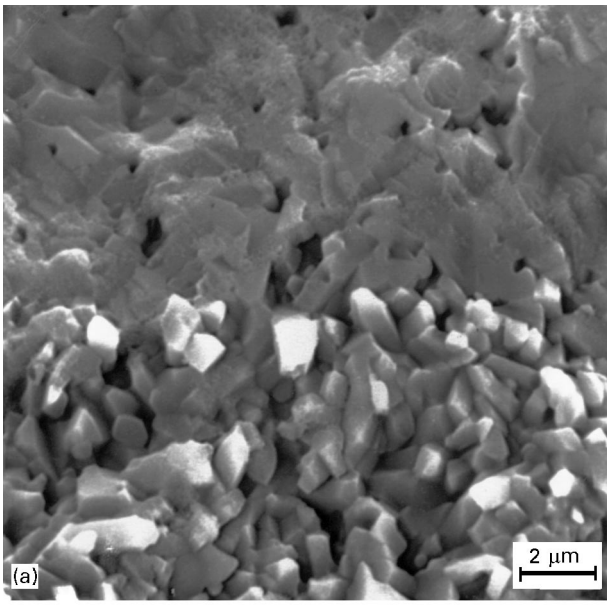

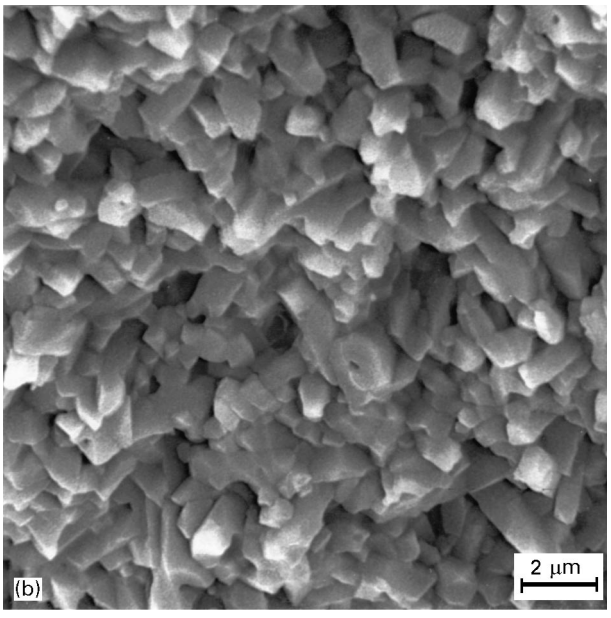

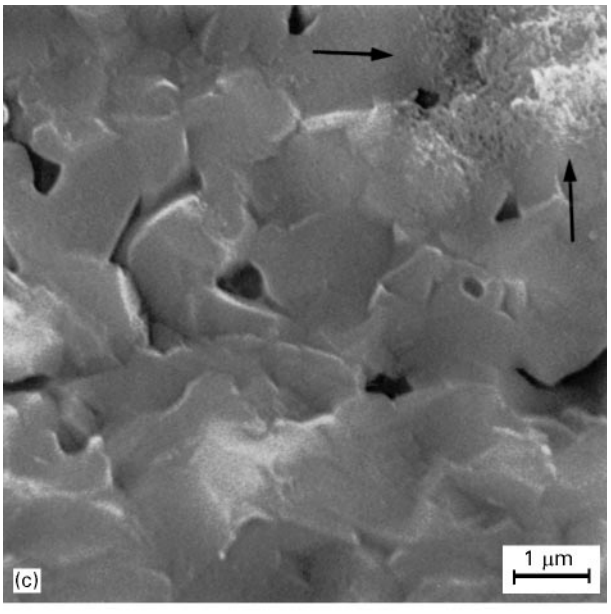

Figure 10 Characteristic features of fracture surfaces of samples tested at 1300 °C using an actuator speed of 0.005 mm min^{-1}. High magnification. (a) Subcritical crack growth zone–sample interphase. (b) Subcritical crack growth zone. (c) Critical fracture zone close to the subcritical crack growth zone.

sample. This kind of microstructure modification (shown in Fig. 6) during fracture has also been observed by other authors around porosity nests in bend samples of a translucent mullite tested at 1400 °C [14] and surrounding defects in creep samples of a high purity mullite [11]. It is interesting to notice that for this feature to be observed in the material studied here, a combination of large defects (i.e. large stress intensities) and long times under load (i.e. low loading rates) is needed.

Toughness values determined at an intermediate loading (0.05 mm min^{-1} equivalent to 194 and 147 N min^{-1} for $E = 171$ and 130 GPa, respectively) increase from temperatures larger than 800 °C as do bend strength values (Figs 4a and 7a). However, crack healing cannot be the only mechanism playing a role here as the evolution of K_{IC} values with loading rate (Fig. 7b) is different from that of bend strength (Fig. 4b). Even though high temperature K_{IC} values are larger than the room temperature ones at all loading rates, the trend that they follow with loading rate is opposite to that shown by materials in which plastic deformation during fracture is an energy absorbing mechanism and leads to larger values of the mechanical parameters for lower loading rates. The K_{IC} fracture surfaces of these samples (Figs 8 and 9) show slow crack growth zones close to the notch, in which intergranular fracture and cavitation occur as in the bend strength samples in which large defects and long times under load are combined (Fig. 6).

Slow crack growth at high temperature in ceramics is commonly related to the presence of a secondary glassy phase. In the regime of temperatures and stresses that this phenomenon occurs, two different processes take place [14]: plastic deformation by grain boundary sliding and reduction of crack-tip stress intensity in the plastic zone by energy dissipation through plastic deformation occurring in the viscous glassy phase. The dominance of grain boundary sliding in materials containing low viscosity silicate glasses produces very fast slow crack growth resulting in a decrease in strength. High viscosity glasses minimize the contribution of grain boundary sliding to strength and the dominance of energy dissipation at the crack tip over grain boundary sliding results in an apparent strengthening of the material. The former of these processes is a weakening one whereas the latter is energy consuming. Grain boundary sliding in materials with no or small amounts of glass is accommodated by cavitation as observed in this mullite (Figs 6c and 9c) and reported by other authors for mullite creep [11, 13]. This weakening process will be minimized for high loading rates, as occurs for samples tested at rates between 0.01 and 5 mm min^{-1} in which the size of subcritical crack growth areas decreases and K_{IC} values increase as loading rate increases (Fig. 8). The "toughening" process is usually more effective for low loading rates but, due to the low viscosity of the liquid formed in the material studied here, this energy dissipative mechanism does not dominate over grain boundary sliding for low loading rates. Moreover, in the mullite studied here, viscosity of the liquid will decrease as time under load increases (as discussed in Section 4.1), improving grain boundary sliding versus crack tip yielding. In fact, in bend strength samples, subcritical crack growth zones are only observed when long times under stress (i.e. low loading rates) are added to large defects (i.e. large stress intensities) (Fig. 6).

The above discussion does not include toughness samples tested using the lowest strain rate, as they should be the weakest and slow crack growth zones in these samples should be the largest. Conversely, slow crack growth zones in these samples are the smallest (Figs 9 and 10) and K_{IC} values are the largest (Fig. 7b). The microstructural changes observed close to the notch at the fracture surfaces of these samples (Fig. 10) might be responsible for this behaviour. Solution–precipitation and/or crystallization phenomena at the crack tip will act as sintering mechanisms during fracture, leading to the observed increase in toughness.

5. Conclusions

Small quantities of alkalis in a $3Al_2O_3 \cdot 2SiO_2$ stoichiometric structural mullite concentrate at the remaining glassy phase. Alkali amount in the glassy phase is orders of magnitude larger than in the average composition of the material.

The mechanical behaviour of a $3Al_2O_3 \cdot 2SiO_2$ stoichiometric structural mullite with 0.2 wt % alkaline impurities and small grain size has been studied from room temperature up to 1400 °C. The main characteristics are the following:

1. Mechanical behaviour at room temperature is linear at all loading rates used and no subcritical crack growth takes place.
2. Mechanical behaviour at high temperature is determined by the residual glassy phase which softens during testing.
3. Mechanical behaviour at high temperature strongly depends on loading rate and stress concentration due to the different processes that take place during heating or testing:

(a) Crack healing takes place during heating.
(b) Decohesion of grains and liquid migration take place during testing, leading to a weakening of the material when low loading rates are added to large stress concentrations.
(c) Very long times under load lead to microstructural modifications that increase toughness values.

Acknowledgements

This work has been supported by CICYT, Project no. MAT 499-91. The authors wish to thank Dr M. I. Osendi for helpful discussions.

References

1. S. SOMIYA and Y. HIRATA, *Ceram. Bull.* **70** (1991) 1624.
2. M. D. SAKS, H. W. LEE and J. A. PASK, in Mullite and mullite matrix composites", Ceramic Transactions, edited by S. Somiya, R. F. Davis and J. A. Pask, Vol. 6 (The American Ceramic Society Inc., USA, 1990) p. 167.

3. H. SCHNEIDER, K. OKADA and J. A. PASK, "Mullite and mullite ceramics" (John Wiley & Sons Ltd., Chichester, 1994) p. 105.
4. C. BAUDIN, M. I. OSENDI and J. S. MOYA, *J. Mater. Sci. Lett*. **2** (1983) 185.
5. C. BAUDIN, P. MIRANZO and M. I. OSENDI, in "Third Euro-Ceramics V-3" (Faenza Editrice Ibérica S.L, Spain, 1993) p. 369.
6. E. F. OSBORN and A. MUAN, in "Phase Diagrams for Ceramists" (The American Ceramics Society Inc., USA, 1964) plate no. 501.
7. G. URBAIN, F. CAMBIER, M. DELETTER and M. R. ANSEAU, *Trans. J. Br. Ceram. Soc*. **80** (1981) 139.
8. J. M. FERNANDEZ NAVARRO, "El vidrio" (Consejo Superior de Investigaciones Científicas, Spain, 1991) p. 337.
9. P. A. LESSING, R. S. GORDON and K. S. MAZDIYASNI, *J. Amer. Ceram. Soc*. **58** (1975) 149.
10. P. C. DOKKO, J. A. PASK and K. S. MAZDIYASNI, *ibid*. **60** (1977) 150.
11. Y. OKAMOTO, H., FUKUDOME, K., HAYASHI and T. NISHIKAWA, *J. Eur. Ceram. Soc*. **6** (1990) 161.
12. A. P. HYNES and R. H. DOREMUS, *J. Amer. Ceram. Soc*. **74** (1991) 2469.
13. M. ASHIZUKA, T. HONDA and Y. KUBOTA, *J. Ceram. Soc. Jpn. Int. Edition* **99** (1991) 282.
14. T. I. MAH and K. S. MAZDIYASNI, *J. Amer. Ceram. Soc*. **66** (1983) 699.
15. Y. YAMADE, Y. KAWAGUCH, N. TAKEDA and T. KISHI, *J. Ceram. Soc. Jpn. Int. Edition* **99** (1991) 452.
16. S. KANZAKI, H. TABATA, T. KUMAZAWA and S. OHTA, *J. Amer. Ceram. Soc*. **68** (1985) C-6.
17. M. G. M. U. ISMAIL, Z. NAKAI and S. SOMIYA, *ibid*. **70** (1987) C7.
18. H.OHNISHI, K. MAEDA, T. NAKAMURA and T. KAWANAMI, in "Mullite and mullite matrix composites", Ceramic Transactions, edited by S. Somiya, R. F. Davis and J. A. Pask, Vol. 6 (The American Ceramic Society Inc., USA, 1990) p. 605.
19. M. MIZUNO, M. SHIRAISHI, H. SAITO, in "Mullite and mullite matrix composites", Ceramic Transactions, edited by S. Somiya, R. F. Davis and J. A. Pask, Vol. 6 (The American Ceramic Society Inc., USA, 1990) p. 413.
20. M. MIZUNO, *J. Amer. Ceram. Soc*. **74** (1991) 3017.
21. T. KUMAZAWA, S., OHTA, T., NAGAOKA and M. YASUOTA, *J. Ceram. Soc. Jpn. Int. Edition* **99** (1991) 1191.
22. T. KUMAZAWA, S. OHTA, S. KANZAKI and H. TABATA, in "Mullite and mullite matrix composites", Ceramic Transactions, edited by S. Somiya, R. F. Davis and J. A. Pask, Vol. 6 (The American Ceramic Society Inc., USA, 1990) p. 401.
23. H. SCHNEIDER, K. OKADA and J. A. PASK, "Mullite and mullite ceramics" (John Wiley & Sons Ltd., Chichester, 1994) p. 199.
24. T. KUMAZAWA, S. KANZAKI, S. OTHA and H. TABATA, *J. Ceram. soc. Jpn*. **96**(1) (1988) 85.
25. G. K. BANSAL, *J. Amer. Ceram. Soc*. **59** (1976) 87.
26. C. R. CHEESEMAN and G. W. GROVES, *J. Mater. Sci*. **20** (1985) 2614.
27. C. RIEF and K. KROMP, "Mechanical testing of engineering ceramics at high temperatures" (Elsevier Applied Science, The Netherlands, 1989) p. 209.
28. I. ODA, M. MATUI and T. SOWA, "Progress in nitrogen ceramics" (Martinus Nijhoff Publisher, The Netherlands, 1983) p. 501.
29. K. KRIZ, in "Progress in nitrogen ceramics" edited by F. L. Riley (Martinus Nijhoff Publisher, The Netherlands, 1983).

Received 19 January
and accepted 31 July 1996